THE JOURNAL OF PHYSICAL CHEMISTRY C

pubs.acs.org/JPCC Article

Ca Cobaltites as Potential Cathode Materials for Rechargeable Ca-Ion Batteries: Theory and Experiment

Haesun Park, Yanjie Cui, Sanghyeon Kim, J. T. Vaughey, and Peter Zapol*

Cite This: J. Phys. Chem. C 2020, 124, 5902−5909 Read Online

ACCESS | Metrics & More | Article Recommendations | Supporting Information

ABSTRACT: Rechargeable Ca-based batteries can potentially achieve higher energy capacity than Li-ion batteries. The development of Ca-ion batteries, however, remains in its infancy, especially due to the challenge of finding cathode materials with high reversible capacity. We investigate properties of Ca cobaltites as Ca-ion intercalation cathodes, by means of density functional theory calculations validated by synthesis and electrochemical measurements. Computationally, we accessed thermodynamic, diffusion properties, energy capacity, and the voltage profiles for four Ca cobaltite compounds of different stoichiometry and Co oxidation states: $Ca_3Co_2O_6$, $CaCo_2O_4$, $Ca_2Co_2O_5$, and $[Ca_2CoO_3][CoO_2]_{1.62}$. We found good stability and relatively low migration barriers of some Ca cobaltites during cycling with the layered $CaCo_2O_4$ having the lowest Ca migration barrier of 0.7 eV and the highest theoretical capacity. To validate our calculations, we synthesized $Ca_3Co_2O_6$, $CaCo_2O_4$, and $[Ca_2CoO_3][CoO_2]_{1.62}$ with the Pechini method and, subsequently, to test the electrochemical extraction of Ca.

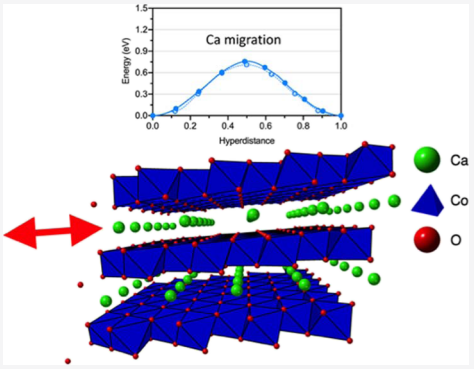

INTRODUCTION

The Ca-ion battery (CIB) technology offers the promise for higher energy density than its more studied alternative based on magnesium.[1] The standard reduction potential of Ca is larger than that of Li only by 170 meV; so a higher cell potential is achievable for a Ca-based cell when compared to a similar Mg-based cell, which has a reduction potential of 670 meV versus Li/Li^+.[2] Moreover, the lower polarizing character of Ca^{2+} entails a faster reaction kinetics than Mg^{2+}.[3] However, the development of CIBs has remained in a very nascent stage.[4]

Recent studies on Ca-based system metallic anode materials have resulted in the isolation of conditions that permit reversible plating of Ca. As with many metallic anodes, the performance of a Ca anode is controlled by the passivating layer on the anode; therefore, the strategies for improving the performance focus on mitigating the parasitic effect at the solid-electrolyte interface. Ponrouch et al. reported successful plating and stripping Ca in 0.45 MM $Ca(BF_4)_2$ ethylene carbonate (EC): propylene carbonate (PC) electrolytes up to 30 cycles.[5] Wang et al. used $Ca(BH_4)_2$ in the tetrahydrofuran electrolyte and observed a large amount of plating (1 mA h cm^{-2} at a rate of 1 mA cm^{-2}) and cyclability (50 cycles).[6] Recently, alloying type anodes based on Sn were demonstrated to enable a high voltage (4.45 V) CIB with exceptional cyclability and 95% capacity retention after 350 cycles at room temperature.[7] Also, recent studies reported calcium tetrakis-(hexafluoroisopropyloxy)borate $Ca[B(hfip)_4]_2$-based electrolytes capable of reversible Ca plating and stripping at room temperature with an anodic stability up to 4.5 V.[8,9]

While some successes have been recently reported for Ca-metal anodes, there have been many efforts to identify Ca-ion cathode materials. The extraction of Ca from TaN_2 was reported, but reinsertion was not successful.[10] The reversible storage of Ca cations has been reported in the layered δ-V_2O_5 framework[11] and various Prussian blue analogues.[12] Recently, several reports indicate that cobalt oxide materials may be able to reversibly intercalate Ca.[11,13] In parallel, computational efforts have resulted in predictions of promising Ca-ion cathode materials with high energy capacity and Ca^{2+} mobilities. In the literature, sulfide spinel compounds have been identified to be promising for Ca-ion cathode materials balancing the cation mobility, thermodynamic stability, and energy capacity.[14,15] Also, the fast Ca ion kinetics in the layered MoO_3 frameworks was predicted from first-principles calculations,[16] but the conversion reaction and the slow diffusion at deep discharge still need to be addressed.[17,18] Recently, α-MnO_2 and layered $TiSe_2$ were computationally assessed as Ca cathode materials, and they showed fast cation kinetics with migration barriers of 0.2 and 0.4 eV, respectively.[19,20] However, in both studies, the evaluation of

Received: December 2, 2019
Revised: February 2, 2020
Published: February 19, 2020

https://dx.doi.org/10.1021/acs.jpcc.9b11192
J. Phys. Chem. C 2020, 124, 5902−5909

the stability of Ca-intercalated compounds was not performed, and the accessible voltages were below 2 V.

Calcium cobaltites represent a class of materials that has been investigated in several studies. The layered $CaCo_2O_4$ structure (also described as $Ca_{0.5}CoO_2$) has been reported as a cathode material for the CIB, which utilized V_2O_5 as an anode.[11] The layered structure was reported to cycle up to 40 times, and the X-ray photoelectron spectra confirmed the redox reaction of Co^{3+}/Co^{4+}. Given that the cation-removed $LiCoO_2$-layered compound, which is a structural analogue of the $CaCo_2O_4$-layered compound, is stable,[21,22] we expect that the layered calcium cobaltites are stable upon charging. Another calcium cobaltite, $Ca_3Co_2O_6$, was reported for the Ca extraction from this class of material, and it was claimed that the unique 1D Ca channels between the cobalt oxide chains facilitate the cation kinetics.[13] An observed phase transformation of $Ca_3Co_2O_6$ during Ca extraction is reasonably well described by the incommensurate modulated structure with Ca and CoO_3 chains having a different periodicity. Other known calcium cobalt oxide materials with an average oxidation state of 3+ include a brownmillerite structure, $Ca_2Co_2O_5$, and related oxygen-deficient perovskite stoichiometries,[23] which have not been evaluated as the intercalation cathode. The perovskite $CaCoO_3$, where the oxidation state of Co is 4+, was investigated previously as a potential cathode material by density functional theory (DFT) calculations, but the Ca migration barrier was over 2 eV.[24]

In addition to materials with Co in the 3+ state described by a general formula $Ca_nCo_2O_{n+3}$, we are interested in incommensurate layered structures with a general formula $(Ca_2CoO_3)(CoO_2)_{1.62}$ that have alternating hexagonal CoO_2 layers and rocksalt-type Ca_2CoO_3 layers. While well known for its thermoelectric properties, this system was not, to our knowledge, investigated as a Ca cathode. Several features have been identified to be potentially interesting from the fundamental point of view. Electrical conductivity is high because one of the sublattices is metallic. The incommensurate structure will keep biaxial distortion primarily confined to the rocksalt layers during cycling with potentially better mechanical stability provided by the CoO_2 layers. The incommensurate structure will make ordering of Ca ions less likely, which in principle could lower diffusion barriers. Additionally, distortions of the rocksalt layer could be beneficial for the distribution of activation energies because of the inequivalence of Ca cations. To the best of our knowledge, no attempt to electrochemically extract Ca from the misfit structure has been made and neither the misfit compound with Ca removed has been reported. A recent computational study addressed the theoretical energy density and the cation diffusion properties for $Ca_3Co_2O_6$, $Ca_3Co_4O_9$, and $Ca_2Co_2O_5$ as Ca-ion cathode materials.[25] In this report, we compare our results for these properties to the ones calculated in the study[25] and assess crucial factors for cathode materials that include phase stability upon cycling and the voltage profiles.

Here, we systematically probe the four different structures and stoichiometries of calcium cobaltites ($Ca_3Co_2O_6$, $CaCo_2O_4$, $Ca_2Co_2O_5$, and $[Ca_2CoO_3][CoO_2]_{1.62}$) for calcium-ion cathode materials. We used DFT calculations to evaluate the thermodynamic stabilities, theoretical energy capacity, voltage behavior, and diffusion properties of calcium cobaltites. In addition, we successfully synthesized several of the target calcium cobaltites ($Ca_3Co_2O_6$, $CaCo_2O_4$, and $[Ca_2Co_3][CoO_2]_{1.62}$) and measured their preliminary electrochemical properties and compared them with the calculation results.

METHODS

DFT[26] calculations as implemented in the Vienna Ab initio Simulation Package[27−29] were used for the electronic structure calculations. The projector-augmented wave[30,31] potentials was used to treat the core−valence electron interactions, and the cutoff energy was set to 520 eV. The generalized gradient approximation (GGA) method developed by Perdew−Burke−Ernzerhof (PBE)[32] was adopted to describe the exchange−correlation functionals. The unphysical delocalization of d-electrons with GGA functional was remedied by adding a Hubbard U correction[33] to the redox active transition metal species, Co(U = 3.32 eV).[34] The Γ-point centered k-point sampling scheme was used in combination with k-point meshes of 3 × 3 × 1 ($Ca_3Co_2O_6$), 2 × 2 × 2 ($CaCo_2O_4$), and 4 × 2 × 2 ($Ca_2Co_2O_5$) and 3 × 3 × 1 ($[Ca_2CoO_3][CoO_2]_{3/2}$), 3 × 3 × 1 ($[Ca_2CoO_3][CoO_2]_{5/3}$), and 3 × 1 × 1 ($[Ca_2CoO_3]$-$[CoO_2]_{5/8}$).

The precise representation of the incommensurate structure for DFT calculations is not possible within the supercell approach. As in our previous work,[35] we approximate the composition ratio of two subsystems by Fibonacci numbers because the experimental ratio is very close to the golden ratio $\varphi = (1 + \sqrt{5})/2 \approx 1.618$ which is the limit of the sequence of the consecutive Fibonacci numbers. Calculated structures for different x/y in (CoO_2) $(Ca_2CoO_3)_{x/y}$ included 3/2, 5/3, and 8/5 approximants and are in good agreement with previous theoretical and experimental studies, for example, 8/5 lattice constants are 0.4 to 1.5% larger than the experimental values. Electronic and magnetic properties are also well-reproduced.[35]

Thermodynamic stabilities are accessed by constructing a phase diagram of the Ca−Co−O ternary system. The concept of the convex hull was used to probe the stability of the ternaries of interest. Pymatgen code was used for the construction of the phase diagram and the calculation of energies above the convex hull.[36] The averaging cell voltage was calculated from the energy difference between charged and discharged states.[37,38] The average voltage can be given by[15,39]

$$\bar{V} = \frac{\Delta G}{nz} \approx \frac{\Delta E}{nz} = \frac{E_{\text{chg.}} + nE(\text{Ca}) - E_{\text{dischg.}}}{nz} \quad (1)$$

where ΔG is the free energy of intercalation reaction. We approximate the free energy by the internal energy, ΔE, because of the small entropic contribution in low temperature. $E_{\text{chg.}}$ and $E_{\text{dischg.}}$ are the total energies of charged and discharged compounds; E(Ca) is the energy of fcc Ca metal per atom; n is the number of Ca ions involved in the intercalating reaction; and z is the charge state of Ca (+2).

In a similar vein, the voltage profile was calculated by evaluating the energy changes with variation of the Ca concentration between charged and discharged phases. The internal energies of charged and discharged phase were used as the relative energy reference to calculate the formation energy of calcium cobalt oxide with an intermediate Ca content. If we assume the chemical formula of the charged and discharged phases to be $Ca_{nc}Ca_aO_b$ and $Ca_{nd}Ca_aO_b$, respectively, then the formation energy of the phase with the intermediate Ca content of x can be expressed as

https://dx.doi.org/10.1021/acs.jpcc.9b11192
J. Phys. Chem. C 2020, 124, 5902−5909

Table 1. Synthesis Parameters for Ca Cobaltites Including Precursors and Calcination Temperatures

reactants	$CaCo_2O_4$	$Ca_3Co_4O_9$	$Ca_2Co_2O_5$	$Ca_3Co_2O_6$
mole ratio $Ca/Co/C_6H_8O_7/C_2H_6O_2$	1:2:3:6	1.5:2:3.5:7	1:1:2:4	3:2:5:10
$Ca(NO_3)_2$ (1.00 M)/mL	10.0	15.0	15.0	30.0
$Co(NO_3)_2$ (1.00 M)/mL	20.0	20.0	15.0	20.0
citric acid ($C_6H_8O_7$)g	6.30	7.36	6.30	10.50
ethylene glycol ($C_2H_6O_2$)g	3.72	4.34	3.72	6.25
calcination temperature °C/time h	600/85 (twice)	800/35	900/60	950/85

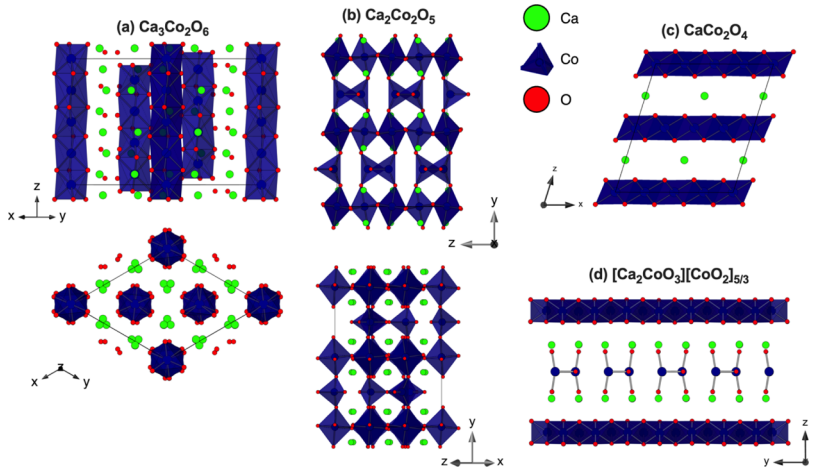

Figure 1. Ball-stick images of considered calcium cobalt oxides (a) $Ca_3Co_2O_6$, (b) $Ca_2Co_2O_5$, (c) $CaCo_2O_4$, and (d) $[Ca_2CoO_3][CoO_2]_{5/3}$. The green, blue, and red spheres represent the Ca, Co, and O atoms, respectively.

$$E_f(Ca_xCo_aO_b) = E(Ca_xCo_aO_b) - \left(\frac{nc - x}{nd - nc}\right)E(Ca_{nc}Co_aO_b) - \left(\frac{x - nc}{nd - nc}\right)E(Ca_{nd}Co_aO_b) \quad (2)$$

where E refers to the internal or DFT total energy and x ranges from nc to nd. The thermodynamic stability of intermediate phases is assessed by comparing their formation energies with the reference phase on the lower convex hull.

From the formation energy convex hull, we can evaluate the piecewise voltage profile by calculating the equilibrium voltage between neighboring stable intermediate phases. The equilibrium voltage between two neighboring intermediate phases with Ca contents of x_1 and x_2, respectively, can be written as

$$V(x_1, x_2) = -\frac{E(Ca_{x_1}Co_aO_b) - E(Ca_{x_2}Co_aO_b) - (x_1 - x_2)E(Ca)}{(x_1 - x_2)ze}, \quad \text{where } x_1 > x_2 \quad (3)$$

The Ca-ion migration barriers in the cobaltite frameworks were evaluated by the nudged elastic band (NEB) method with a climbing image scheme[40] using GGA−PBE functional without the U correction, as suggested in previous work.[15] This is because the metastability of the electronic structure along the cation migration path causes difficulty in converging the climbing image NEB calculations.[15] Also, there is no clear evidence that the inclusion of Hubbard correction improves the accuracy in predicting the cation migration barriers.[41−44]

Experimental Methods. Each material was synthesized using the Pechini method.[45] All starting materials were purchased from Sigma-Aldrich with purities ranging from 98 to 99.8% ($Ca(NO_3)_2{\cdot}4H_2O$, 99% $Co(NO_3)_2{\cdot}6H_2O$, 98% citric acid anhydrous, 99.5%, ethylene glycol, 99.8%). For each composition, a stoichiometric mixture of metal nitrates was dissolved in water and placed in a beaker on a magnetic stirrer and heated to about 70 °C to remove excess water and promote esterification of the citric acid with the ethylene glycol. As water evaporates, the solution became more viscous; the gel was transferred to a 6 L fused silica beaker. The temperature was raised to promote the decomposition of the polymer (see Table 1). The nitrate residue causes partial oxidation of the organic groups. This highly exothermic process is self-sustaining, and the polymer transforms into a highly porous black powder. Calcination of the materials in high temperature furnaces under air was used to calcine the samples and crystallize the product. Ratios and temperatures for each composition are shown in Table 1.

Characterization Studies. Phase purity was determined by powder X-ray diffraction methods on the dried samples using a Bruker D8 Diffraction system. Samples were compared to the ICSD database standards. The materials $CaCo_2O_4$, $Ca_3Co_4O_9$, and $Ca_3Co_2O_6$ were found to be single phase to powder X-ray diffraction. The brownmillerite composition, $Ca_2Co_2O_5$, was found, under the conditions used, to be a physical mixture of CaO, $Ca_3Co_2O_6$, and $Ca_3Co_4O_9$. Literature studies have indicated that a more oxidizing environment, for instance, a pure oxygen atmosphere, is required to create the desired phase.[23]

As a baseline complete cell for evaluating Ca-ion cathodes is yet to be standardized, the materials were tested against a Ca-metal or Sn-metal anode using 0.5 M $Ca(TFSI)_2$ and EC/PC solvent mixture. The PC was dried with 4 A molecule sieves before use, and EC was used directly. The $Ca(TFSI)_2$ salt was dried before use. The positive electrode was prepared by first mixing a slurry containing 80 wt % active material, 10 wt % carbon black, and 10 wt % polyvinylidene fluoride binder,

https://dx.doi.org/10.1021/acs.jpcc.9b11192
J. Phys. Chem. C 2020, 124, 5902−5909

previously dissolved in *N*-methyl-2-pyrrolidinone (NMP), and a proper amount of NMP as the dispersant. The slurry was then coated on an aluminum foil using a doctor blade. The NMP was removed by first drying the electrode at 75 °C for 2 h and then further drying the electrode in a vacuum oven at 100 °C overnight. The active material loading is about 1.6 mg/cm^2. A half-cell was constructed in an argon-filled glove box. The separator was a Celgard 2325 film. The cells were tested with a MACCOR electrochemical analyzer at a current density of 10 mA/g with various voltage windows. Electrochemical tests were conducted at room temperature and duplicated to check reproducibility.

RESULTS AND DISCUSSION

Figure 1 depicts the structure of four different calcium cobaltite compounds considered in this study. In Figure 1a, which is the structure of $Ca_3Co_2O_6$, the octahedral and trigonal prismatic geometries of CoO_6 are alternatively connected in the z direction forming unique 1D chains. The Ca atoms are positioned along the 1D channel surrounded by three neighboring CoO_6 chains. The facile diffusion of Ca ion along these channels is expected.[13] The structure of brownmillerite $Ca_2Co_2O_5$ is plotted in Figure 1b. The Co atoms are coordinated either octahedrally or tetrahedrally along the long axis of the unit cell. The $CaCo_2O_4$ and incommensurate ($[Ca_2CoO_3][CoO_2]_{5/3}$) layered structures are shown in Figure 1c,d, respectively. We tested different chemical compositions $[Ca_2CoO_3][CoO_2]_x$ (x = 3/2, 5/3, and 8/5), and their lattice parameters are compared with experimental values in Figure S1 and Table S1. The structures with x =5/3 and 8/5 reproduce experimental structural properties within 3.5%, and we selected x = 5/3 composition balancing the structure representation and affordable simulation cell size.

The charged phase was obtained by removing the Ca atoms from the discharged state up to the 4+ oxidation state of Co. For example, the oxidation state of Co in $CaCo_2O_4$ is 3+; therefore, the removal of all Ca atoms leads to the oxidation state of Co of 4+, a layered CoO_2. Similarly, the removal of one Ca atom out of three in $Ca_3Co_2O_6$ (to yield $Ca_2Co_2O_5$) results in the change of the oxidation of Co from 3+ to 4+. In the incommensurate $[Ca_2CoO_3][CoO_2]_{5/3}$, the removal of one Ca leads to the oxidation state of Co in the rock-salt subsystem to be 4+. The 50 configurations for distribution of remaining Ca atoms in the charged state are initially generated by minimizing the electrostatic energy using pymatgen code,[36] and they are fully relaxed through DFT calculations. The lowest energy structure was selected as a representative charged structure.

The calculated phase diagram of the Ca−Co−O_2 ternary system is given in Figure 2a. Among the calculated calcium cobaltites, the approximate incommensurate $[Ca_2CoO_3]$-$[CoO_2]_{5/3}$ structure was the most stable ternary compound. Another approximation to the incommensurate structure with the rock-salt/layered mixing ratio of 8/5 was close in stability, with the energy above hull of 0.3 meV/atom, as shown in Figure 2b. Given that there are many reports that this compound has been synthesized,[46] our stability prediction of incommensurate structures agrees with experimental observations. The other three calcium cobaltites, $CaCo_2O_4$ (17 meV/atom), $Ca_3Co_3O_6$ (5 meV/atom), and $Ca_2Co_2O_5$ (9 meV/atom), have energy above hull less than 18 meV, which indicates that these compounds are metastable, but they are all reported to be successfully synthesized.[11,13,23] Note that the

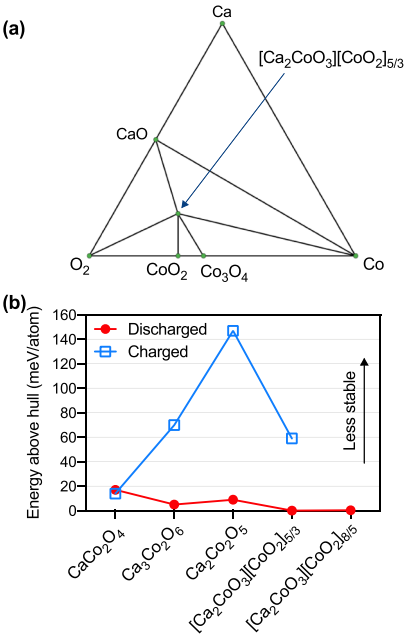

Figure 2. (a) Phase diagram of the Ca−O_2−Co ternary system constructed from DFT calculated energies. (b) Energy above hull of charged and discharged states of calcium cobaltite considered in this study. Here, the discharged phase refers to the structure with a stoichiometry corresponding to a chemical formula on the x-axis, and the charged phase was constructed by removing Ca atoms from the discharged phase up to the oxidation limit of Co (Co IV). Blue (squares) and red (circles) represent the charged and discharged phases.

typical error of the DFT phase stability calculations involving oxides is approximately 24 meV/atom.[47] This could affect determination of stability for the $CaCo_2O_4$, $Ca_3Co_3O_6$, and $Ca_2Co_2O_5$ phases, which have energy above hull within the error threshold.

The stability of charged states that are constructed by removing the Ca atoms up to the oxidation limit of Co is also explored because this property is crucial to probe the cyclability of the cathode. We calculated and plotted the energy above hull of the charged layered-$CaCo_2O_4$, 1D-$Ca_3Co_2O_6$, brownmillerite $Ca_2Co_2O_5$, and incommensurate $[Ca_2CoO_3][CoO_2]_{5/3}$ in Figure 2b. The energy above hull for Co_2O_4, the charged phase of $CaCo_2O_4$, is 14 meV/atom, which is within the error (24 meV/atom) of the DFT phase stability calculations. The spinel $CaCo_2O_4$ counterpart has energy above hull of ∼60 meV/atom in both charged and discharged phases,[15] and thus the layered structure is more suitable for cathode in terms of stability. For $Ca_3Co_2O_6$, $Ca_2Co_2O_5$, and $[Ca_2CoO_3][CoO_2]_{5/3}$; however, the energy above hull for charged states becomes much larger than discharged phases ($Ca_3Co_2O_6$: 5 meV/atom → 70 meV/atom, $Ca_2Co_2O_5$: 9 meV/atom → 147 meV/atom $[Ca_2CoO_3][CoO_2]_{5/3}$: 0 meV/atom → 59 meV/atom). This suggests that $Ca_3Co_2O_6$, $Ca_2Co_2O_5$, and $[Ca_2CoO_3][CoO_2]_{5/3}$ become less stable as extracting Ca, but their chemical decomposition might be kinetically limited.

Table 2 summarizes the average voltage, Ca extraction onset voltage, cell volume at charged/discharged phase, volume change, gravimetric capacity, and specific energy of the considered calcium cobaltite cathode materials. $[Ca_2CoO_3]$-$[CoO_2]_{5/3}$ has the highest average voltage of 3.81 V, and the

https://dx.doi.org/10.1021/acs.jpcc.9b11192
J. Phys. Chem. C 2020, 124, 5902−5909

Table 2. Calculated Average Voltage, Ca Extraction On-Set Voltage, Gravimetric Capacity, Specific Energy, Cell Volume at Charged/Discharged States, and Volume Change of $CaCo_2O_4$, $Ca_2Co_2O_5$, $Ca_3Co_2O_6$, and $[Ca_2CoO_3][CoO_2]_{5/3}$[a]

		$CaCo_2O_4$	$Ca_2Co_2O_5$	$Ca_3Co_2O_6$	$[Ca_2CoO_3][CoO_2]_{5/3}$
average voltage (V)		3.26	3.68	3.32	3.81
Ca extraction on-set voltage (V)	DFT	2.31		3.13	3.60
	experiment	2.5		3.0	3.5
gravimetric capacity (mA h/g)		242	193	160	158
specific energy (W h/kg)		788	710	533	604
volume (Å^3)	discharged	914	884	769	774
	charged	888	863	735	763
volume change (%)		−2.8	−2.3	−4.3	−1.4

[a]The experimentally observed Ca extraction on-set voltages of $Ca_2Co_2O_5$, $Ca_3Co_2O_6$, and $[Ca_2CoO_3][CoO_2]_{5/3}$ are given.

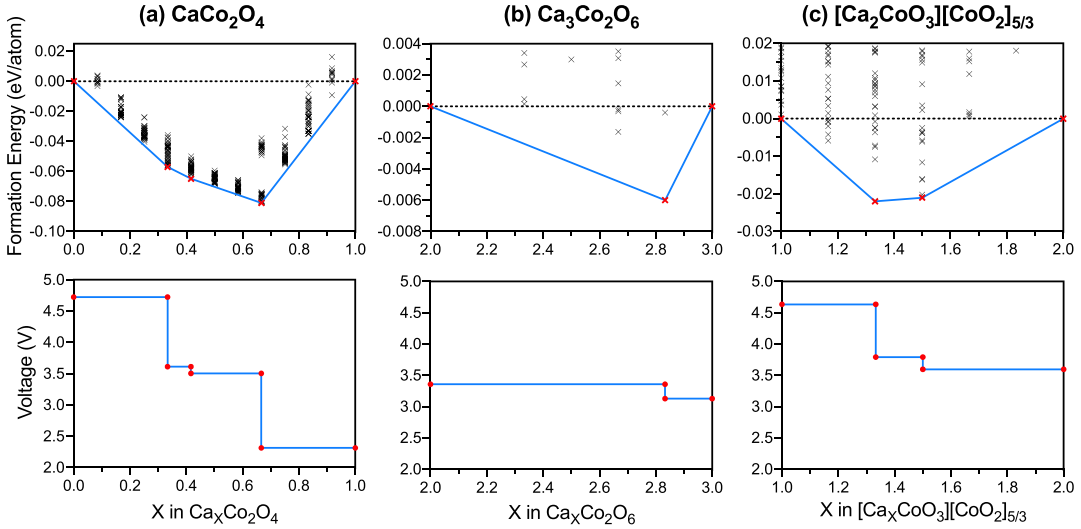

Figure 3. Calculated formation energy convex hull and the voltage profile of (a) $CaCo_2O_4$, (b) $Ca_3Co_2O_6$, and (c) $[Ca_2CoO_3][CoO_2]_{5/3}$.

other two show values that are lower by ∼0.5 V($CaCo_2O_4$, $Ca_3Co_2O_6$) or ∼0.2 V ($Ca_2Co_2O_5$). The spinel cobaltite counterpart shows the average voltage of ∼3.4 V.[15] The theoretical gravimetric capacity of $CaCo_2O_4$ is ∼242 mA h/g, which is comparable to the spinel $CaCo_2O_4$. For $Ca_3Co_2O_6$, $Ca_2Co_2O_5$, and $[Ca_2CoO_3][CoO_2]_{5/3}$, the gravimetric capacity and the corresponding specific energy are lower than layered $CaCo_2O_4$ by 34, 20, and 34%, respectively. This is because the extractable cations are limited compared to the layered structure due to the already high oxidation state Co metal in $Ca_3Co_2O_6$, $Ca_2Co_2O_5$, and $[Ca_2CoO_3][CoO_2]_{5/3}$. The calculated theoretical gravimetric capacities of $Ca_3Co_2O_6$ and $[Ca_2CoO_3][CoO_2]_{5/3}$ are same with the previous report.[25] The maximum volume decrease was approximately 4.3% upon Ca extraction, and this is much lower than the spinel structure, which experiences about 20% decrease.[15]

The first row of Figure 3 shows the DFT formation energies of partially charged states as a function of Ca content X between the charged and discharged phases of $CaCo_2O_4$, $Ca_3Co_2O_6$, and $[Ca_2CoO_3][CoO_2]_{5/3}$. At this point, we exclude $Ca_2Co_2O_5$ from the analysis because of the low stability in the charged state. At least 50 Ca vacancy configurations are considered at each Ca content except at the high and low vacancy limits. As elaborated in eq 2, the formation energies at Ca content of X are referenced to the internal (or DFT) energies of the charged and discharged states. The ground state convex hulls (blue lines) are shaped by connecting the calculated ground state formation energies (red mark). The corresponding voltage profiles are described in the second row of Figure 3. From Figure 3a, three ground states are identified at X = 0.333, 0.417, and 0.667 for $CaCo_2O_4$. The voltage profile shows that the steep voltage changes of ∼1 V occur at X = 0.333 and 0.667. The voltage range calculated using DFT at 0 K is between 2.3 and 4.7 V, which approximately accord with experimental observations.[11] In ref 11, the operating voltage in between −0.3 and +1.6 V versus Ag/AgCl reference electrode was observed during $CaCo_2O_4$ charge/discharge. Given the Ca/Ca^{2+} versus Ag/AgCl is 3.08 V,[2] the operating voltage of $CaCo_2O_4$ is in the range between 2.78 and 4.68 V versus Ca/Ca^{2+}, which is in agreement with our results.

Figure 3b plots the convex hull of $Ca_3Co_2O_6$ and the corresponding voltage profile. One ground state was observed at the Ca content of 2.833. The voltage profile of $Ca_3Co_2O_6$ is relatively flat compared with that of $CaCo_2O_4$, and there was no steep voltage change at the ground state which is the vertices of the convex hull. This is because the voltage change loosely corresponds to the depth of the convex hull.[48] The depth of the convex hull of $Ca_3Co_2O_6$ is approximately an order of magnitude smaller than that of $CaCo_2O_4$ and $[Ca_2CoO_3][CoO_2]_{5/3}$, which entails a moderate voltage shift. The experimental electrochemical charge[13] of $Ca_3Co_2O_6$ occurs in the voltage range between 3.2 and 3.5 V, which is similar to our calculated voltage range (3.1−3.4 V). The convex hull plot of $[Ca_2CoO_3][CoO_2]_{5/3}$ shows two ground

https://dx.doi.org/10.1021/acs.jpcc.9b11192
J. Phys. Chem. C 2020, 124, 5902−5909

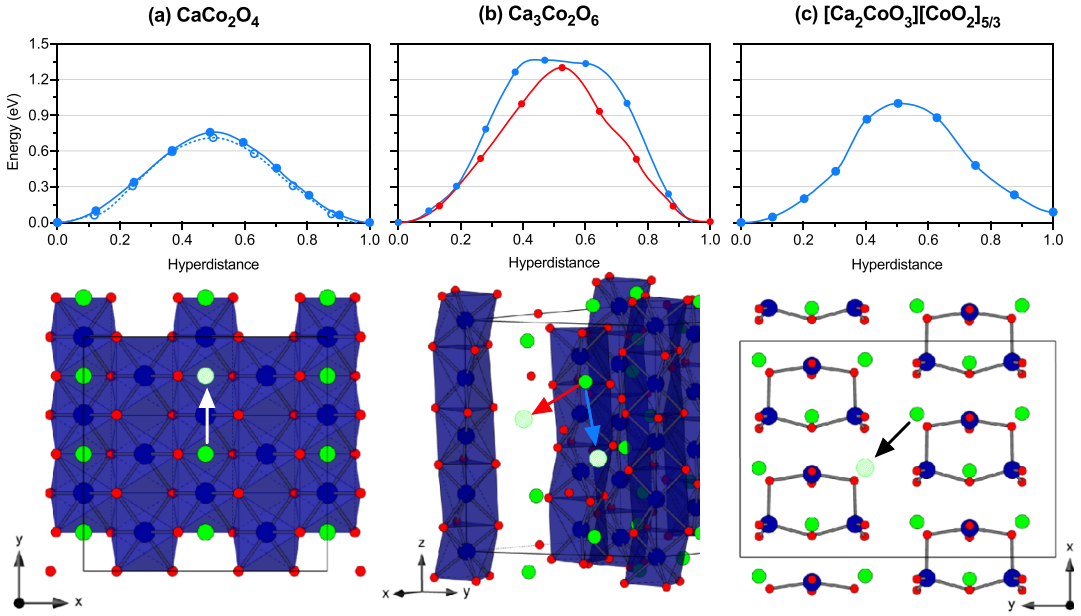

Figure 4. Calculated MEPs for migration (first row) and the schematics of the corresponding migration pathways (second row) of Ca cations in (a) $CaCo_2O_4$, (b) $Ca_3Co_2O_6$, and (c) $[Ca_2CoO_3][CoO_2]_{5/3}$. Solid and dashed lines represent the low and high vacancy limits, respectively. The blue and red color scheme in $Ca_3Co_2O_6$ represent the two different Ca pathways which are the intra- and interchannel diffusion. Green, red, and blue spheres in the second row represent Ca, O, and Co atoms, respectively. The slashed green sphere signifies the Ca vacancy site.

states at $X = 1.333$ and 1.5. The sharp voltage shift takes place only at the Ca content of 1.333, and it drops from 4.6 to 3.8 V.

Single phase samples were synthesized by the Pechini method and annealed in air to crystallize the desired materials, and their X-ray diffraction patterns are given in Figure S2. Three of the samples ($CaCo_2O_4$, $Ca_3Co_2O_6$, and $[Ca_2CoO_3][CoO_2]_{1.62}$) were found to be single phase, while the perovskite-related $Ca_2Co_2O_5$ was found to be a mixture of other ternary phases and calcium oxide. Preliminary electrochemical evaluation was performed using two different reported anodes (Ca, Sn) and a $Ca(TFSI)_2$-based electrolyte in an EC/PC solvent mixture.[49] Initial charging tests showed low activity up to 4.2 V (vs Sn) with approximately 2% of the Ca removed for each composition (Table S2). As shown in Figure S3, data collected showed small initial plateaus consistent with charging of the materials from the cathode surface sites. The open circuit voltage data from these surface charging reactions are consistent with the calculations noted in Figure 3. The on-set voltage calculations well-reproduce not only the absolute values (~0.1 V deviation) but also the tendency that $[Ca_2CoO_3][CoO_2]_{5/3}$ and $CaCo_2O_4$ exhibit the highest and lowest voltages, respectively. Experimentally, however, complete cell discharge was not achievable using present cell designs. Various studies in the literature have highlighted the difficulty in identifying and evaluating CIB cells due to issues associated with calcium stripping and plating and issues arising from poor calcium diffusion through the anode passivation layer.[5] The limited Ca extraction noted experimentally from the cathode can be attributed to the poor kinetics at the anode and the inaccessibility of a low impedance pathway with the current cell design. Attempts to use discharged tin as an anode gave similar results. So we probe the Ca diffusion properties in the tested compound frameworks by means of NEB.

The diffusivity of the working cation is a critical factor to enable the reversible intercalation into the cathode and the diffusion of multivalent cations, which are expected to be more challenging due to the stronger interaction with the anion than that of the single-valent Li ion. So, accessing the kinetic properties of Ca ions in the cobaltite frameworks is critical to finding promising cathode materials. The way to gauge the diffusivity of Ca ions within the cobaltite frameworks is to calculate the minimum energy pathway (MEP) for migration of Ca cations to the nearest vacancy site. The MEPs for $CaCo_2O_4$, $Ca_3Co_2O_6$, and $[Ca_2CoO_3][CoO_2]_{5/3}$ are plotted in Figure 4.

In Figure 4a, the MEPs of Ca in $CaCo_2O_4$ are drawn at the high and low Ca vacancy limits. The migration path of Ca ions between sites is depicted in the second row of Figure 4a. Because of the nature of the layered structure, Ca cations are expected to be mobile in the *xy* plane which is parallel to the CoO_2 layers. Both vacancy concentration limits show a migration barrier of about 0.75 eV, which is the lowest among the tested cobaltites.

In the $Ca_3Co_2O_6$ structure, there can be two Ca migration pathways, and both showed the migration barrier higher than 1.2 eV, as shown in Figure 4b. As discussed in the previous section, the CoO_6 chains build up the 1D channel expanding in the *z*-direction, and Ca cations are located within the channel. So, a Ca cation can hop to the neighboring vacancy site within the 1D channel (intrachannel diffusion) or in the adjacent channels (interchannel diffusion). Both migration pathways require very similar activation energies (intrachannel: 1.36 eV and interchannel: 1.30 eV), as depicted in the first row of Figure 4b, but these energies are much larger than that in the layered $CaCo_2O_4$. The shape of MEP of intrachannel exhibits a small plateau at the saddle point which signifies the diffusion of Ca through the intermediate polyhedral, and this is in agreement with the previous report.[25] However, the migration barriers calculated in this work are approximately 0.4 eV higher than in ref 25, and the discrepancy might occur because the climbing image NEB was not used in the previous study to calculate migration barriers in $Ca_3Co_2O_6$. A recent report suggests that the concerted migration of cations is the origin of

https://dx.doi.org/10.1021/acs.jpcc.9b11192
J. Phys. Chem. C 2020, 124, 5902−5909

low energy barriers in various Li-ion conducting solids.[50] In order not to overlook lower energy pathway, we considered the concerted migration of Ca cations along the 1D channel in the *z*-direction, but the energy barrier was greater than 3 eV.

The diffusion pathway and the corresponding MEP of the Ca cations in the $[Ca_2CoO_3][CoO_2]_{5/3}$ structure is given in Figure 4c. We only considered the diffusion of the Ca cations within the *xy* plane formed by the Ca_2CoO_3 rock-salt and the CoO_2 layers. The diffusion exhibits the energy barrier of about 1.00 eV which is still very sluggish, and it is in accordance with the previous report.[25]

CONCLUSIONS

The thermodynamic stability analysis accessed by phase diagram construction confirmed that the discharged phases of $Ca_3Co_2O_6$, $CaCo_2O_4$, and $[Ca_2CoO_3][CoO_2]_{1.62}$ are in the thermodynamically stable range (*E* above hull <50 meV). However, in case of $Ca_2Co_2O_5$, while it is thermodynamically stable in the discharged state (*E* above hull = 9 meV), the energy above hull rises to 147 meV in the charged state equivalent to full calcium extraction, and the structure becomes unstable. The voltage behaviors of $Ca_3Co_2O_6$, $CaCo_2O_4$, and $[Ca_2Co_3][CoO_2]_{1.62}$ are calculated by varying the Ca concentration between charged and discharged states. The calculated Ca extraction on-set voltages are well-matched to the experimental observations. The initial electrochemical measurements did not show cycling behavior, which can be attributed to the reactions between the electrolyte and cathode/anode forming undesirable blocking layers, which impedes the electrochemical extraction or insertion of the working cations. Finally, we explored the Ca diffusion in cobaltite frameworks and find that layered $CaCo_2O_4$ exhibit the lowest Ca migration barriers of 0.75 eV, while Ca diffusion in $Ca_3Co_2O_6$ and $[Ca_2CoO_3][CoO_2]_{1.62}$ is expected to be much more sluggish with calculated hopping barriers greater than 1.00 eV. Based on these results, the layered Ca cobaltite is the most promising candidate Ca-ion cathode material of the studied compounds in terms of stability, capacity, and mobility. Given that the layered structure is one of the most common structure types of materials for Li, Na, and Mg-ion cathodes, further investigations for the layered materials are required to unlock their intrinsic electrochemical properties as a Ca-ion intercalation cathode.

ASSOCIATED CONTENT

Supporting Information

The Supporting Information is available free of charge at https://pubs.acs.org/doi/10.1021/acs.jpcc.9b11192.

Crystal structures; lattice parameters; X-ray diffraction patterns; and synthesis parameters (PDF)

AUTHOR INFORMATION

Corresponding Author

Peter Zapol − *Joint Center for Energy Storage Research (JCESR) and Materials Science Division, Argonne National Laboratory, Lemont, Illinois 60439, United States;* orcid.org/0000-0003-0570-9169; Email: zapol@anl.gov

Authors

Haesun Park − *Joint Center for Energy Storage Research (JCESR) and Materials Science Division, Argonne National Laboratory, Lemont, Illinois 60439, United States;* orcid.org/0000-0001-6266-8151

Yanjie Cui − *Joint Center for Energy Storage Research (JCESR) and Chemical Sciences and Engineering Division, Argonne National Laboratory, Lemont, Illinois 60439, United States*

Sanghyeon Kim − *Joint Center for Energy Storage Research (JCESR) and Chemical Sciences and Engineering Division, Argonne National Laboratory, Lemont, Illinois 60439, United States*

J. T. Vaughey − *Joint Center for Energy Storage Research (JCESR) and Chemical Sciences and Engineering Division, Argonne National Laboratory, Lemont, Illinois 60439, United States;* orcid.org/0000-0002-2556-6129

Complete contact information is available at: https://pubs.acs.org/10.1021/acs.jpcc.9b11192

Notes

The authors declare no competing financial interest.

ACKNOWLEDGMENTS

This work was supported as part of the Joint Center for Energy Storage Research, an Energy Innovation Hub funded by the U.S. Department of Energy, Office of Science, Basic Energy Sciences. The work at Argonne National Laboratory was performed under contract no. DE-AC02-06CH11357. We acknowledge grants of computer time from ANL Laboratory Computing Resource Center (LCRC).

REFERENCES

(1) Ponrouch, A.; Palacin, M. R. On the road toward calcium-based batteries. *Curr. Opin. Electrochem.* **2018**, *9*, 1−7.

(2) Vanýsek, P. Electrochemical Series. In *CRC Handbook of Chemistry and Physics*, 100th ed.; Rumble, J., Ed.; CRC Press LLC, 2019.

(3) Muldoon, J.; Bucur, C. B.; Gregory, T. Quest for Nonaqueous Multivalent Secondary Batteries: Magnesium and Beyond. *Chem. Rev. (Washington, DC, U.S.)* **2014**, *114*, 11683−11720.

(4) Arroyo-de Dompablo, M. E.; Ponrouch, A.; Johansson, P.; Palacín, M. R. Achievements, Challenges, and Prospects of Calcium Batteries. *Chem. Rev.* **2019**, DOI: 10.1021/acs.chemrev.9b00339.

(5) Ponrouch, A.; Frontera, C.; Bardé, F.; Palacín, M. R. Towards a calcium-based rechargeable battery. *Nat. Mater.* **2016**, *15*, 169.

(6) Wang, D.; Gao, X.; Chen, Y.; Jin, L.; Kuss, C.; Bruce, P. G. Plating and stripping calcium in an organic electrolyte. *Nat. Mater.* **2018**, *17*, 16.

(7) Wang, M.; Jiang, C.; Zhang, S.; Song, X.; Tang, Y.; Cheng, H.-M. Reversible calcium alloying enables a practical room-temperature rechargeable calcium-ion battery with a high discharge voltage. *Nat. Chem.* **2018**, *10*, 667−672.

(8) Li, Z.; Fuhr, O.; Fichtner, M.; Zhao-Karger, Z. Towards stable and efficient electrolytes for room-temperature rechargeable calcium batteries. *Energy Environ. Sci.* **2019**, *12*, 3496−3501.

(9) Shyamsunder, A.; Blanc, L. E.; Assoud, A.; Nazar, L. F. Reversible Calcium Plating and Stripping at Room Temperature Using a Borate Salt. *ACS Energy Lett.* **2019**, *4*, 2271−2276.

(10) Verrelli, R.; Black, A. P.; Frontera, C.; Oró-Solé, J.; Arroyo-de Dompablo, M. E.; Fuertes, A.; Palacín, M. R. On the Study of Ca and Mg Deintercalation from Ternary Tantalum Nitrides. *ACS Omega* **2019**, *4*, 8943−8952.

(11) Cabello, M.; Nacimiento, F.; González, J. R.; Ortiz, G.; Alcántara, R.; Lavela, P.; Pérez-Vicente, C.; Tirado, J. L. Advancing towards a veritable calcium-ion battery: CaCo2O4 positive electrode material. *Electrochem. Commun.* **2016**, *67*, 59−64.

(12) Lipson, A. L.; Pan, B.; Lapidus, S. H.; Liao, C.; Vaughey, J. T.; Ingram, B. J. Rechargeable Ca-Ion Batteries: A New Energy Storage System. *Chem. Mater.* **2015**, *27*, 8442−8447.

(13) Tchitchekova, D. S.; Frontera, C.; Ponrouch, A.; Krich, C.; Bardé, F.; Palacín, M. R. Electrochemical calcium extraction from 1D-Ca3Co2O6. *Dalton Trans.* **2018**, *47*, 11298−11302.
(14) Liu, M.; Jain, A.; Rong, Z.; Qu, X.; Canepa, P.; Malik, R.; Ceder, G.; Persson, K. A. Evaluation of sulfur spinel compounds for multivalent battery cathode applications. *Energy Environ. Sci.* **2016**, *9*, 3201−3209.
(15) Liu, M.; Rong, Z.; Malik, R.; Canepa, P.; Jain, A.; Ceder, G.; Persson, K. A. Spinel compounds as multivalent battery cathodes: a systematic evaluation based on ab initio calculations. *Energy Environ. Sci.* **2015**, *8*, 964−974.
(16) Rong, Z.; Kitchaev, D.; Canepa, P.; Huang, W.; Ceder, G. An efficient algorithm for finding the minimum energy path for cation migration in ionic materials. *J. Chem. Phys.* **2016**, *145*, 074112.
(17) Tojo, T.; Tawa, H.; Oshida, N.; Inada, R.; Sakurai, Y. Electrochemical characterization of a layered α-MoO3 as a new cathode material for calcium ion batteries. *J. Electroanal. Chem.* **2018**, *825*, 51−56.
(18) Cabello, M.; Nacimiento, F.; Alcántara, R.; Lavela, P.; Pérez Vicente, C.; Tirado, J. L. Applicability of Molybdite as an Electrode Material in Calcium Batteries: A Structural Study of Layer-type CaxMoO3. *Chem. Mater.* **2018**, *30*, 5853−5861.
(19) Juran, T. R.; Smeu, M. TiSe2 cathode for beyond Li-ion batteries. *J. Power Sources* **2019**, *436*, 226813.
(20) Juran, T. R.; Young, J.; Smeu, M. Density Functional Theory Modeling of MnO2 Polymorphs as Cathodes for Multivalent Ion Batteries. *J. Phys. Chem. C* **2018**, *122*, 8788−8795.
(21) Tarascon, J. M.; Vaughan, G.; Chabre, Y.; Seguin, L.; Anne, M.; Strobel, P.; Amatucci, G. In Situ Structural and Electrochemical Study of Ni1−xCoxO2 Metastable Oxides Prepared by Soft Chemistry. *J. Solid State Chem.* **1999**, *147*, 410−420.
(22) Shimoda, K.; Murakami, M.; Takamatsu, D.; Arai, H.; Uchimoto, Y.; Ogumi, Z. In situ NMR observation of the lithium extraction/insertion from LiCoO2 cathode. *Electrochim. Acta* **2013**, *108*, 343−349.
(23) Zhang, J.; Zheng, H.; Malliakas, C. D.; Allred, J. M.; Ren, Y.; Li, Q. a.; Han, T.-H.; Mitchell, J. F. Brownmillerite Ca2Co2O5: Synthesis, Stability, and Re-entrant Single Crystal to Single Crystal Structural Transitions. *Chem. Mater.* **2014**, *26*, 7172−7182.
(24) Arroyo-de Dompablo, M. E.; Krich, C.; Nava-Avendaño, J.; Palacín, M. R.; Bardé, F. In quest of cathode materials for Ca ion batteries: the CaMO3 perovskites (M = Mo, Cr, Mn, Fe, Co, and Ni). *Phys. Chem. Chem. Phys.* **2016**, *18*, 19966−19972.
(25) Torres, A.; Bardé, F.; Arroyo-de Dompablo, M. E. Evaluation of cobalt oxides for calcium battery cathode applications. *Solid State Ionics* **2019**, *340*, 115004.
(26) Hohenberg, P.; Kohn, W. Inhomogeneous Electron Gas. *Phys. Rev.* **1964**, *136*, B864−B871.
(27) Kresse, G.; Furthmüller, J. Efficient iterative schemes for ab initio total-energy calculations using a plane-wave basis set. *Phys. Rev. B: Condens. Matter Mater. Phys.* **1996**, *54*, 11169−11186.
(28) Kresse, G.; Furthmüller, J. Efficiency of ab-initio total energy calculations for metals and semiconductors using a plane-wave basis set. *Comput. Mater. Sci.* **1996**, *6*, 15−50.
(29) Kresse, G.; Hafner, J. Ab initio molecular dynamics for liquid metals. *Phys. Rev. B: Condens. Matter Mater. Phys.* **1993**, *47*, 558−561.
(30) Blöchl, P. E. Projector augmented-wave method. *Phys. Rev. B: Condens. Matter Mater. Phys.* **1994**, *50*, 17953−17979.
(31) Kresse, G.; Joubert, D. From ultrasoft pseudopotentials to the projector augmented-wave method. *Phys. Rev. B: Condens. Matter Mater. Phys.* **1999**, *59*, 1758−1775.
(32) Perdew, J. P.; Burke, K.; Ernzerhof, M. Generalized Gradient Approximation Made Simple. *Phys. Rev. Lett.* **1996**, *77*, 3865−3868.
(33) Dudarev, S. L.; Botton, G. A.; Savrasov, S. Y.; Humphreys, C. J.; Sutton, A. P. Electron-energy-loss spectra and the structural stability of nickel oxide: An LSDA+U study. *Phys. Rev. B: Condens. Matter Mater. Phys.* **1998**, *57*, 1505−1509.
(34) Wang, L.; Maxisch, T.; Ceder, G. Oxidation energies of transition metal oxides within the GGA+U framework. *Phys. Rev. B: Condens. Matter Mater. Phys.* **2006**, *73*, 195107.
(35) Rébola, A.; Klie, R.; Zapol, P.; Öğüt, S. First-principles study of the atomic and electronic structures of misfit-layered calcium cobaltite (Ca2CoO3)(CoO2)1.62 using rational approximants. *Phys. Rev. B: Condens. Matter Mater. Phys.* **2012**, *85*, 155132.
(36) Ong, S. P.; Richards, W. D.; Jain, A.; Hautier, G.; Kocher, M.; Cholia, S.; Gunter, D.; Chevrier, V. L.; Persson, K. A.; Ceder, G. Python Materials Genomics (pymatgen): A robust, open-source python library for materials analysis. *Comput. Mater. Sci.* **2013**, *68*, 314−319.
(37) Aydinol, M. K.; Ceder, G. First-Principles Prediction of Insertion Potentials in Li-Mn Oxides for Secondary Li Batteries. *J. Electrochem. Soc.* **1997**, *144*, 3832−3835.
(38) Aydinol, M. K.; Kohan, A. F.; Ceder, G.; Cho, K.; Joannopoulos, J. Ab initio study of lithium intercalation in metal oxides and metal dichalcogenides. *Phys. Rev. B: Condens. Matter Mater. Phys.* **1997**, *56*, 1354−1365.
(39) Urban, A.; Seo, D.-H.; Ceder, G. Computational understanding of Li-ion batteries. *npj Comput. Mater.* **2016**, *2*, 16002.
(40) Henkelman, G.; Uberuaga, B. P.; Jónsson, H. A climbing image nudged elastic band method for finding saddle points and minimum energy paths. *J. Chem. Phys.* **2000**, *113*, 9901−9904.
(41) Dathar, G. K. P.; Sheppard, D.; Stevenson, K. J.; Henkelman, G. Calculations of Li-Ion Diffusion in Olivine Phosphates. *Chem. Mater.* **2011**, *23*, 4032−4037.
(42) Ong, S. P.; Chevrier, V. L.; Hautier, G.; Jain, A.; Moore, C.; Kim, S.; Ma, X.; Ceder, G. Voltage, stability and diffusion barrier differences between sodium-ion and lithium-ion intercalation materials. *Energy Environ. Sci.* **2011**, *4*, 3680−3688.
(43) Lin, H.; Wen, Y.; Zhang, C.; Zhang, L.; Huang, Y.; Shan, B.; Chen, R. A GGA+U study of lithium diffusion in vanadium doped LiFePO4. *Solid State Commun.* **2012**, *152*, 999−1003.
(44) Eom, T.; Lim, H.-K.; Goddard, W. A.; Kim, H. First-Principles Study of Iron Oxide Polytypes: Comparison of GGA+U and Hybrid Functional Method. *J. Phys. Chem. C* **2015**, *119*, 556−562.
(45) Cushing, B. L.; Kolesnichenko, V. L.; O'Connor, C. J. Recent Advances in the Liquid-Phase Syntheses of Inorganic Nanoparticles. *Chem. Rev.* **2004**, *104*, 3893−3946.
(46) Masset, A. C.; Michel, C.; Maignan, A.; Hervieu, M.; Toulemonde, O.; Studer, F.; Raveau, B.; Hejtmanek, J. Misfit-layered cobaltite with an anisotropic giant magnetoresistance: ${\mathrm{Ca}}_{3}{\mathrm{Co}}_{4}{\mathrm{O}}_{9}$. *Phys. Rev. B: Condens. Matter Mater. Phys.* **2000**, *62*, 166−175.
(47) Hautier, G.; Ong, S. P.; Jain, A.; Moore, C. J.; Ceder, G. Accuracy of density functional theory in predicting formation energies of ternary oxides from binary oxides and its implication on phase stability. *Phys. Rev. B: Condens. Matter Mater. Phys.* **2012**, *85*, 155208.
(48) Chen, T.; Sai Gautam, G.; Huang, W.; Ceder, G. First-Principles Study of the Voltage Profile and Mobility of Mg Intercalation in a Chromium Oxide Spinel. *Chem. Mater.* **2018**, *30*, 153−162.
(49) Shakourian-Fard, M.; Kamath, G.; Taimoory, S. M.; Trant, J. F. Calcium-Ion Batteries: Identifying Ideal Electrolytes for Next-Generation Energy Storage Using Computational Analysis. *J. Phys. Chem. C* **2019**, *123*, 15885−15896.
(50) He, X.; Zhu, Y.; Mo, Y. Origin of fast ion diffusion in super-ionic conductors. *Nat. Commun.* **2017**, *8*, 15893.

https://dx.doi.org/10.1021/acs.jpcc.9b11192
J. Phys. Chem. C 2020, 124, 5902−5909